



Experimental study on the mechanism of flow blockage formation in fast reactor

Wen-Hui Jin¹ · Song-Bai Cheng¹ · Xiao-Xing Liu¹

Received: 3 December 2022 / Revised: 17 March 2023 / Accepted: 25 March 2023 / Published online: 17 June 2023

© The Author(s), under exclusive licence to China Science Publishing & Media Ltd. (Science Press), Shanghai Institute of Applied Physics, the Chinese Academy of Sciences, Chinese Nuclear Society 2023

Abstract

Various sources of solid particles might exist in the coolant flow of a liquid metal cooled fast reactor (e.g., through chemical interaction between the coolant and impurities, air, or water, through corrosion of structural materials, or from damaged/molten fuel). Such particles may cause flow blockage accidents in a fuel assembly, resulting in a reduction in coolant flow, which potentially causes a local temperature rise in the fuel cladding, cladding failure, and fuel melt. To understand the blockage formation mechanism, in this study, a series of simulated experiments was conducted by releasing different solid particles from a release device into a reducer pipe using gravity. Through detailed analyses, the influence of various experimental parameters (e.g., particle diameter, capacity, shape, and static friction coefficient, and the diameter and height of the particle release nozzle) on the blockage characteristics (i.e., blockage probability and position) was examined. Under the current range of experimental conditions, the blockage was significantly influenced by the aforementioned parameters. The ratio between the particle diameter and outlet size of the reducer pipe might be one of the determining factors governing the occurrence of blockage. Specifically, increasing the ratio enhanced blockage (i.e., larger probability and higher position within the reducer pipe). Increasing the particle size, particle capacity, particle static friction coefficient, and particle release nozzle diameter led to a rise in the blockage probability; however, increasing the particle release nozzle height had a downward influence on the blockage probability. Finally, blockage was more likely to occur in non-spherical particles case than that of spherical particles. This study provides a large experimental database to promote an understanding of the flow blockage mechanism and improve the validation process of fast reactor safety analysis codes.

Keywords Liquid metal cooled fast reactor · Flow blockage · Granular jamming · Experimental study

1 Introduction

The disaster in March 2011 at the Fukushima Dai-Ichi nuclear power plant in Japan highlights that severe accidents are bound to occur, despite their extremely low probability [1–3]. Liquid metal cooled fast reactors (LMFRs)

are competitive next-generation nuclear reactors with higher safety, stronger economic competitiveness, and less nuclear waste than their predecessors and offer effective prevention of nuclear proliferation [4–6]. The literature has suggested that flow blockage is one of the initiators that leads to severe accidents in LMFRs [7, 8]. LMFRs are designed to operate in a single phase. The presence of a secondary phase (e.g., solid particles) negatively affects coolant flow and heat transfer. Generally, the accumulation of solid particles accounts for the presence of a secondary phase, which causes a so-called flow blockage accident. There are various sources of solid particles, for example, foreign materials left after construction, chemical interactions between coolant and impurities, air or water, debris released from cladding failure, and the spacer wire loosening or breaking. The flow blockage in the subchannel (i.e., partial or total obstruction) can lead to a reduction

This work was supported by the Basic and Applied Basic Research Foundation of Guangdong Province (Nos. 2021A1515010343 and 2022A1515011582) and the Science and Technology Program of Guangdong Province (Nos. 2021A0505030026 and 2022A0505050029).

✉ Song-Bai Cheng
chengsb3@mail.sysu.edu.cn

¹ Sino-French Institute of Nuclear Engineering and Technology, Sun Yat-Sen University, Zhuhai 519082, China

in coolant flow and, thus, cause a potential degradation of heat transfer and an increase in temperature, which might eventually result in the local cladding failure and a fuel melt [9]. Therefore, safety analyses are imperative. The main purpose of safety research is to evaluate the effects of blockages on the cooling of the fuel pins and neighboring fuel pins.

There are two types of flow blockages in LMFRs: planar blockage (mainly relevant for grid-spaced fuel bundles) and porous blockage (typically emerging in wire-wrapped fuel bundles), according to Van Tichelen [10]. She presents a detailed overview of the latest international activities in this field. She also summarized and assessed experimental and theoretical studies on blockages. Generally, the thermal–hydraulic effects caused by flow blockages are determined by the size and thermal-physical properties of the blockage, coolant flow rate, fuel pin power, and location of the blockage. The magnitude of the overall flow reduction is generally small unless the blockage is large, which makes it difficult to detect the occurrence of a local blockage. However, in theory, a reduction in the coolant flow causes an increase in the temperature. According to the literature, an increase in the average core outlet temperature or fluctuation in radioactivity in the reactor can be used as a warning or signal [11, 12].

Conventionally, researchers have used thermal–hydraulic system codes to conduct numerical analyses of flow blockages. Nowadays, numerical research benefits from the availability of modern simulation methods, namely, computational fluid dynamics (CFD), which makes acquiring detailed knowledge before conducting concrete experiments possible. Di Piazza et al. [13] conducted a CFD analysis for the Advanced Lead Fast Reactor European Demonstrator fuel assemblies in the case of flow blockage with slightly overloaded conditions. Researchers have found that flow blockage has two major effects: a local effect in the wake region behind the blockage and a global effect in the blocked subchannels. Sarkar et al. [14] proposed a porous body model considering the total flow blockage in a fuel subassembly of seven and 19 bare pin fuel bundles. They found that regardless of the differences in power input, the maximum sodium temperature trapped in the blocked subassembly reaches the sodium boiling point. To model the temperature and velocity fields inside a wire-wrapped fuel assembly under blocked and unblocked conditions, Di Piazza et al. [15] and Marinari et al. [16] each performed a three-dimensional thermal–hydraulic analysis of the fuel assembly. Their studies investigated different flow blockage regimes, namely, blockages at various locations and of different extensions in a 19 pins fuel bundle. Their findings demonstrated that all general trends in the temperature and velocity fields in the wrapped fuel assembly were fully captured by the modeling approaches.

In addition to numerical simulations, experimental studies have been conducted. Pacio et al. [17] investigated the thermal–hydraulic effects under specific scenarios (i.e., two small blockages covering one central and another edge subchannel, and a large blockage covering six subchannels). The experimental results showed that in all cases, there was a significant temperature increase at the mid-height of the blockage elements, and small blockages might be acceptable from a safety perspective, but large blockages would likely result in clad failure. Marinari et al. [18] conducted experimental tests to simulate thermal–hydraulic characteristics in a flow blockage scenario in a natural circulation experiment loop-upgraded facility. Their experimental results showed two major effects of the blockage: a local effect with a maximum temperature behind the blockage and an overall effect with a local peak temperature at the end of the active region in the blocked subchannels.

The aforementioned studies mainly concentrated on the impact of flow blockage under reactor conditions (i.e., the result of blockage). However, equally crucial is to study the process of particle accumulation (i.e., the process of blockage or the reason for blockage). The subsequent section focuses on research on the development of a typical blockage event in various industries, namely, the food storage and pharmaceutical industries. For example, Kiwing et al. [19] conducted an experiment on the blockage phenomenon by releasing monodisperse disks into two-dimensional hoppers and attempted to explain the blockage probability quantitatively. Many experimental studies on jamming during the discharge of particles from a silo have also been performed to further analyze the avalanche size distribution (a size used to quantitatively describe the blockage probability), the existence of a critical radius (a size that guarantees a complete absence of blockage), and the effect of particle properties on blockage [20, 21]. However, the experimental conditions and the research priorities of these studies generally differ from those of blockage studies of LMFRs fuel assemblies.

The literature has focused on the impact of flow blockage but paid little attention to the process of its formation. Many of the experimental conditions, namely, the size, axial position, and radial position of the blockage, have been set without full consideration or appropriate explanations. Understanding the accumulation process of solid particles would improve the understanding of the occurrence of flow blockage accidents and their mechanisms, a systematic project comprising a series of experiments in three well-organized stages was initiated at Sun Yat-Sen University.

In the first stage, a reducer pipe was used to simulate the fuel assembly subchannel. Subsequently, a certain number of solid particles of various diameters, densities, capacities, and static friction coefficients were released from the device into the reducer pipe by gravity. The main aim of this stage

was to clarify the effect of particle properties on the blockage formation mechanisms, thereby obtaining knowledge of the blockage phenomenon that would be useful in complicated scenarios. In addition to experimental analyses, predictive model studies and numerical calculations (e.g., using the discrete element method) were conducted simultaneously. In the second stage, a real subchannel structure with a more complicated geometry than that in the first stage was used to conduct additional simulated experiments and numerical investigations. In the third stage, a liquid loop with an upward flow was constructed, and a core subassembly geometry was included to simulate a flow blockage accident under a more realistic flow scenario than that in the first and the second stage. This study focused on the experimental activities of the first stage. Knowledge and fundamental data from our work can also be used for predictive model studies and for conducting analyses and validations of fast reactor safety analysis codes.

2 Experimental setup

Figure 1a shows the experimental facility used in this study. The facility comprises a stainless steel support to sustain the release device, a reducer pipe, and a scissor lift table to adjust the height of the reducer pipe. The other equipment was a video cassette recorder that recorded the experimental process and a backlight. The experimental process was as follows:

At the beginning of each experimental run, a certain number of solid particles was accurately counted and loaded into the particle release device, a stainless steel conical hopper. Additionally, to eliminate the ill effects caused by the dispersion of solid particles from the reducer pipe during their free falling, columniform pipes with inner diameters of 30 and 45 mm were connected to the bottom of the particle release device. Next, we pulled the plug upward using a string. Finally, the particles stored in the hopper were released and fell into the reducer pipe under gravity, and the digital video camera recorded the entire process of particle fall and blockage (if any). A backlight was used behind the reducer pipe to improve the observation quality. Further qualitative observations and quantitative measurements were conducted using image analysis software to analyze the images extracted from the video recordings.

To simulate the formation of a flow blockage accident in the subchannel of LMFRs, we first investigated and calculated the equivalent hydraulic diameters of subchannels in typical fast reactors worldwide [15, 17, 22, 23]. Next, we connected the fuel pin diameter, fuel pin pitch, and equivalent hydraulic diameter of the central subchannel of representative reactors and found that the equivalent diameter of the subchannels in these reactors mostly varied from 3

to 13 mm [24]. To broaden the applicability, as shown in Fig. 1a, we designed a reducer pipe with an inner diameter ranging from 3 to 50 mm and a height of 1000 mm to simulate the subchannel in the fuel assembly. This diameter range covered the majority of the subchannel sizes of the statistical subchannel dimensions. However, in reactor cases, subchannels are not reducer pipes. Notably, we employed a reducer pipe in this study because the premier target of our Stage I project was the effect of particle properties (rather than the subchannel shape) on blockage formation mechanisms, and a reducer pipe is convenient for acquiring efficient data on the effects of the parameters. To improve the visual observation and photography, we used transparent quartz glass as the material for the reducer pipe.

Regarding the simulant of obstruction particles, little is known about the properties (e.g., size and shape) of obstruction particles because the sources of particles vary, and available data are rare [9]. Therefore, in this study, to understand their parametric effects, particle properties were determined based on a comprehensive evaluation, namely, cost, representativeness, and sufficiency. For example, to clarify the effect of the particle size, five different sizes with a wide range (i.e., 0.2–8 mm) were utilized. For the particle shape, two types of non-spherical particles with different characteristics were used. To provide evidence on the influence of the surface roughness of solid particles, we also considered particles with different static friction coefficients (details are summarized in the following paragraph). In addition, particles of different capacities were utilized to investigate the effect of particle number density on the blockage process. Finally, release devices of different sizes and heights were employed to study the influence of release conditions on the blockage.

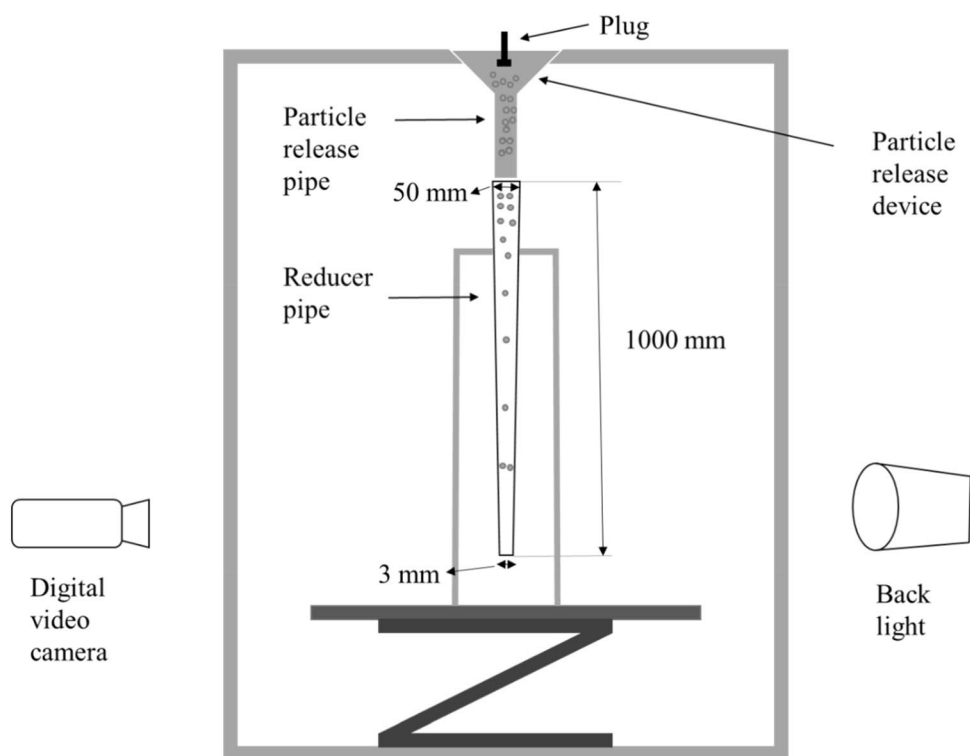
To obtain the general characteristics of the flow blockage behavior, various experimental parameters, namely, particle size (d_p), particle capacity (C_p), particle static friction coefficient (μ_p), particle shape, particle release pipe diameter (D_{pipe}), and particle release height (H_p), were used. Table 1 summarizes the specific physical properties of the solid particles and the experimental conditions. Figure 1b shows representative particles of different shapes and materials. The volume-equivalent diameters of the cylindrical aluminum and triangular prism were obtained from Cheng et al. [25].

3 Experimental analyses and discussion

3.1 Overview of the main experimental phenomena

Figure 2 shows the complete blockage process in a typical experiment. The keyframes were extracted using a digital video camera. First, the particles were released from a certain height, as shown in Fig. 2a. Next, several particles

Fig. 1 (Color online) Experimental equipment and materials. **a** Experimental facility used in this work. The upper diameter, lower diameter, and height of the reducer pipe are 3, 50, and 1000 mm, respectively. **b** An image of some representative spherical and non-spherical particles



(a)



Alumina particles
(sphere, $d_v=6$ mm)



Steel particles
(sphere, $d_v=6$ mm)



Aluminium particles
(sphere, $d_v=6$ mm)



Alumina particles
(triangular prism, $d_v=3.58$ mm)



Glass particles
(sphere, $d_v=6$ mm)



Aluminium particles
(cylinder, $d_v=5.62$ mm)

(b)

passed through the marked expected location successively (because the particles that moved separately would not cause a blockage here) and stopped at the final location (because the particle diameter was 4 mm and it should stop in the reducer pipe section with a diameter of 4 mm) as shown from Fig. 2a–e. Above these particles there were two particles denoted as particle left and particle right): particle left was almost parallel to particle right, as shown in Fig. 2f. As shown in Fig. 2g, h, when these two parallel particles passed through the expected location, they

stopped and formed an arch (which was comprised of two particles and was mentioned in Kiwing et al. [19]). After the arch was formed, the subsequent particles stopped and were blocked above the arch, as shown in Fig. 2i, j. An interspace below the arch was observed because of its occurrence. This blockage event was typical in our research, suggesting that the blockage was the result of the formation of an arch in a certain place, which supports Kiwing's analysis. Notably, in our experiments, the arch always consisted of two particles, whereas in Kiwing's

Table 1 Detailed conditions of our runs performed using spherical and non-spherical particles

| Material (density kg/m ³) | Shape | d_v (mm) | Static friction coefficient | D_{pipe} (mm) | H_p (mm) | Particle capacity (number) |
|---------------------------------------|------------------|------------|-----------------------------|------------------------|------------|-----------------------------|
| Glass 2600 | Sphere | 0.2 | 0.266 | 45 | 280 | 62 |
| | | 0.5 | | 45 | 280 | 62 |
| | | 2 | | 45 | 280 | 62 |
| | | 4 | | 45 | 280 | 62 |
| | | 6 | | 30 | 280 | 62, 123, 186, 245, 490, 613 |
| | | | | 45 | 280 | 62, 123, 186, 245, 490, 613 |
| | | | | 45 | 765 | 62, 123, 245, 490, 613 |
| | | | | 45 | 280 | 62 |
| Aluminum 2700 | Sphere | 6 | 0.474 | 30 | 280 | 62, 123, 186, 245, 490, 613 |
| | | | | 45 | 280 | 62, 123, 186, 245, 490, 613 |
| | | | | 45 | 765 | 62, 123, 186, 245, 490 |
| | Cylinder | 5.62 | - | 30 | 280 | 62 |
| | | | | 45 | 280 | 62 |
| | | | | 45 | 765 | 62 |
| Alumina 3600 | Sphere | 4 | 0.547 | 45 | 280 | 62 |
| | | 6 | | 30 | 280 | 62, 123, 186, 245, 490, 613 |
| | | | | 45 | 280 | 62, 123, 186, 245, 490, 613 |
| | | | | 45 | 765 | 62, 123, 186, 245, 490 |
| | Triangular prism | 3.58 | - | 30 | 280 | 62 |
| | | | | 45 | 280 | 62 |
| | | | | 45 | 765 | 62 |
| Steel 7900 | Sphere | 6 | 0.330 | 30 | 280 | 62, 123, 186, 245, 490, 613 |
| | | | | 45 | 280 | 62, 123, 186, 245, 490 |
| | | | | 45 | 765 | 62, 123, 186, 245, 490 |

study, the arch comprised 2–7 particles. The reason for this phenomenon remains unclear. Thus, an inference could be that this difference might be closely correlated to the experimental conditions, especially the reducer pipe’s angle (the angle in our experiment was approximately 88.7°, and the angles in Kiwing’s experiment were 34°, 60°, and 75°) and its dimensions (the reducer pipe used in our experiment was a three-dimensional pipe, and that of Kiwing’s experiment was a two-dimensional hopper).

3.2 Analyses of experimental parameters

As indicated in Sect. 3.1, the formation of an arch in the reducer pipe is a key indicator for evaluating the occurrence of flow blockage. The main purpose of the following section is to achieve a general understanding of the effect of the experimental parameters on the probability of the formation of an arch (P_{arch}) (also called jamming probability). The jamming probability is obtained as N_b/N_t , where N_t is the number of trials for each case (in this study, each case was repeated 100 times), and N_b is the number of blockage trials.

3.2.1 Effect of particle size

Figure 3 shows the variation in the jamming probability (P_{arch}) with particle size. As shown in Fig. 3, with an increase in the particle size, the jamming probability increases sharply (from 0) and then tends to approach a constant value. When the particle size was smaller than 0.5 mm, jamming did not occur. These results are consistent with those reported by Arnold et al. [26], Drescher et al. [27], Jenike et al. [28], and Walker et al. [29]. In these studies, the critical ratio of the outlet size to the particle size R_c (which guarantees the absence of jamming) was mentioned. The critical outlet size was approximately 5–10 times the particle size of the non-cohesive particles. In this study, the outlet size of the reducer pipe was 3 mm, which is six times the 0.5 mm size. We reasonably expected that the particles with a diameter less than 0.5 mm would not block the reducer pipe. When the particle size increased, an arch started to form, and jamming occurred. In addition, the jamming probability remained virtually unchanged when the particle size was larger than 2 mm. Notably, the ratio of particle size to jamming section size (R) is regarded as the most influential variable for determining the jamming probability [30]. In

Fig. 2 (Color online) Image of a typical blockage event (Stainless steel spherical particles, $d_p = 4$ mm, $C_p = 123$ particles, $D_{\text{pipe}} = 45$ mm, $H_p = 280$ mm). Red ellipse contains the particles moving separately. Two blue arrows point to the marked expected position and final position. Two yellow arrows point to particle left and particle right under blockage. Purple circle is the interspace

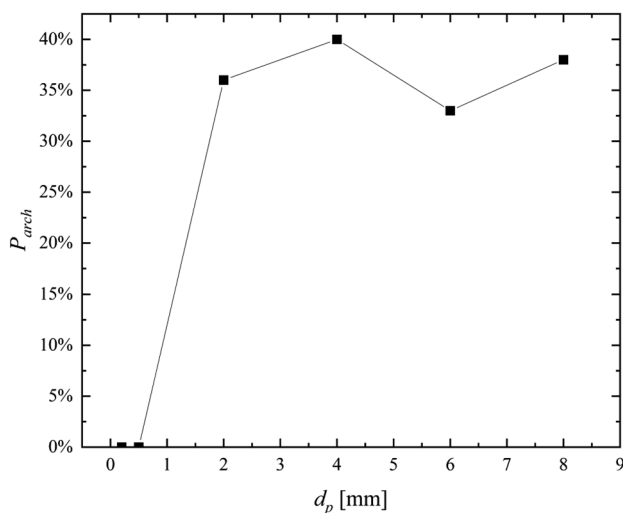
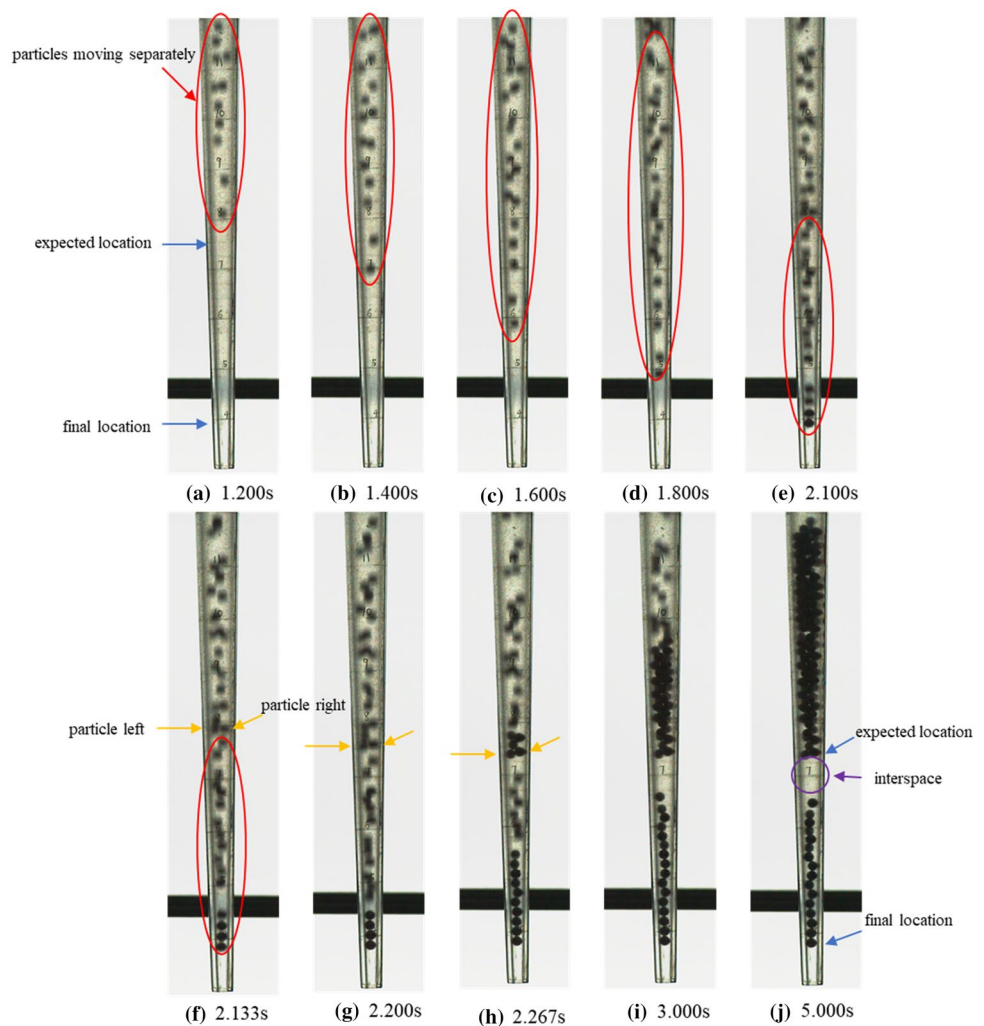


Fig. 3 Effect of particle size on jamming probability for glass (Spherical particles, $d_p = 0.2$ –8 mm, $C_p = 62$ particles, $D_{\text{pipe}} = 45$ mm, $H_p = 280$ mm). The line is a guide to the points only

most studies, when R decreases, the mean avalanche size decreases (the avalanche size is defined as the number of particles flowing out of the reducer pipe before an arch forms and has a straightforward connection with P_{arch} [31]). In all the blockage cases shown in Fig. 3, the arches are in a section whose diameter is approximately two times the particle diameter; thus, the ratio R remains unchanged. Therefore, a reasonable assumption is that the jamming probability remains stable as the particle size increases. Notably, the jamming probability is not 100%. This finding is normal because except for the ratio R , jamming is affected by the morphology of the exit, the particle number density, and other properties of the particles [19].

3.2.2 Effect of particle static friction coefficient

Among the physical properties of a particle, the surface roughness (herein, the static friction coefficient is a suitable parameter) is a key factor in the formation of an arch [19]. To clarify how friction plays a role in jamming probability,

researchers have repeated experiments on two types of particles with almost the same density (2600 kg/m^3 and 2700 kg/m^3) but different static friction coefficients (for glass $\mu_p = 0.266$ and for aluminum $\mu_p = 0.474$). The friction coefficients were tested using a friction coefficient tester, in which 200 g of particles were pulled by a force with a velocity of 100 mm/min. The particle materials used were glass and aluminum with the same particle size $d_p = 6 \text{ mm}$.

Figure 4a–c depict the effects of the particle static friction coefficient on P_{arch} for different particle capacities (C_p), particle release pipe diameters (D_{pipe}), and particle release heights (H_p). P_{arch} of the rough particle (aluminum) is always larger than that of the smooth particle (glass). Evidently, a larger static friction coefficient probably support an increase in friction in the contact between two particles and between the particle and wall, increasing the ease with which an arch can form; thus, jamming occurs. This finding is consistent with those of To et al. [19], Pournin et al. [32], and Pugnaroni et al. [33]. According to their research, an increase in friction causes an increase in jamming possibilities because tangential forces play a significant role in the stability of the arch system. Therefore, a reasonable assumption is that static friction increases, jamming probability increases.

3.2.3 Effect of particle capacity

To investigate the influence of particle capacity on jamming probability, we conducted experiments with different numbers of particles. The experiment was repeated 100 times for each case. The particle materials used were glass and aluminum with the same particle size, $d_p = 6 \text{ mm}$.

Figure 4d–f present the variation in jamming probability with the particle capacity for distinct particle release pipe diameters (D_{pipe}) and at various particle release heights (H_p). These graphs show that the jamming probability increases as the number of particles in the particle release device increases. Owing to the increasing particle number, the particle number density in the entire reducer pipe increased (particularly above the arch), which made the particles sufficiently close to each other, decreasing the velocity of the particles above the jamming section. Under these circumstances, if the ratio of outlet size to particle size is smaller than R_c , jamming may appear [34]. Therefore, the jamming probability increases with an increase in particle capacity. These findings agree with those of Hou et al. [35], who illustrated that the phenomenon of crowding could be understood as a transition from dilute to dense flow and that jamming is a transition from dense flows to a jammed phase. Notably, when the particle number density increases, the opportunities for particles to collide with each other increase; in other words, the particle number density increases, the jamming probability increases.

3.2.4 Effect of particle release pipe diameter

The effect of the particle release pipe diameter on the jamming probability for 6 mm stainless steel particles and alumina particles is shown in Fig. 5a, b. As shown in Fig. 5a, b, as pipe diameter increases, jamming probability increases. Notably, when the release pipe diameter increases, the number of particles entering the reducer pipe per second increases. Thus, the particle flow increases, resulting in the growth of the particle number density above the arch and finally an increase in jamming probability. This analysis is consistent with the effect of the particle capacity, both of which confirm the significance of the particle number density above the jamming. Moreover, in our trial experiments with release pipe diameters less than 20 mm (not listed in Table 1), when particles with a diameter of 6 mm passed through such a narrow release pipe, they were easily blocked in the releasing pipe or completely interrupted the particle flow, which further supports the existence of a critical ratio of outlet size to particle diameter R_c (5–10). Therefore, our blockage experiments were conducted in releasing pipes with particle diameters greater than 30 mm.

3.2.5 Effect of particle release height

Figure 5c, d illustrate the effect of the particle release height on the jamming probability for the stainless steel (6 mm) and alumina (6 mm) particles; as shown in these graphs, when H_p increased from 280 to 765 mm, P_{arch} decreased slightly. The change in jamming probability is largely due to the following: when the particles are released from a high place, the particles become more divergent than that released from low place, that is, the particle number density in the entire reducer pipe decreases. Notably, in a free fall, when particles are released one after another, the vertical distance between the two particles increases according to the free fall law. This phenomenon explains why the particles released from high place became more divergent than that released from low place. Consequently, the chance of particles colliding with each other decreases, which decreases the jamming probability. Another contributing factor is that increasing the particle release height might increase the velocity of particles above the arch. In other words, particles' momentum would increase, resulting in the formed arch being stricken more heavily than that formed in case of low place. Subsequently, the arch becomes less stable during the collision of the particles above the arch. As a result of these two effects, the jamming probability decreases as the particle release height increases.

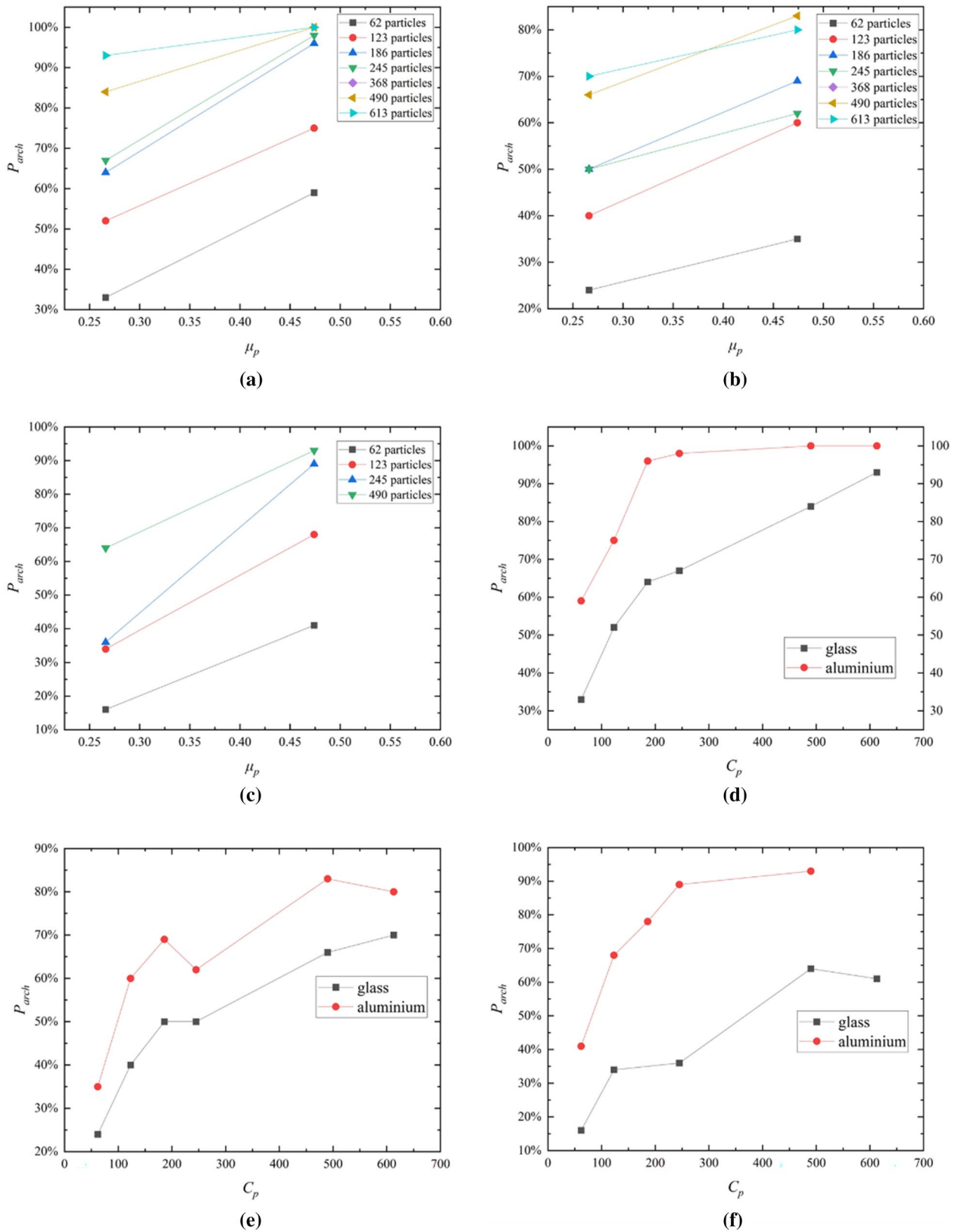


Fig. 4 Influence of static friction coefficient and particle capacity on P_{arch} for glass and aluminium. **a** $D_{pipe}=45$ mm, $H_p=280$ mm. **b** $D_{pipe}=30$ mm, $H_p=280$ mm. **c** $D_{pipe}=45$ mm, $H_p=765$ mm.

d $D_{pipe}=45$ mm, $H_p=280$ mm. **e** $D_{pipe}=30$ mm, $H_p=280$ mm. **f** $D_{pipe}=45$ mm, $H_p=765$ mm

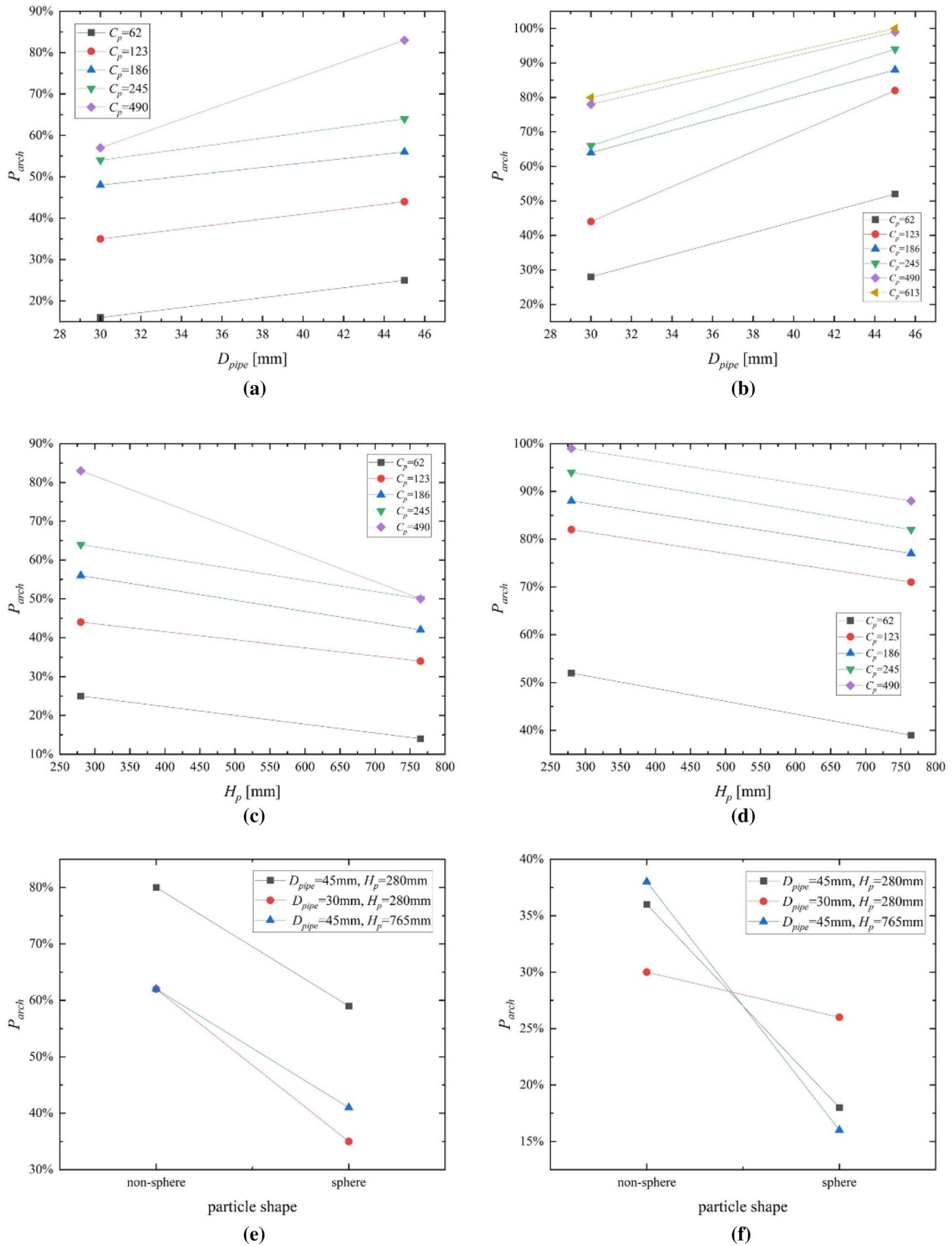


Fig. 5 Influence of particle release pipe diameter, release height, and particle shape on P_{arch} . **a** stainless steel particle with $d_p=6$ mm and $H_p=280$ mm. **b** alumina particle with $d_p=6$ mm and $H_p=280$ mm. **c**

stainless steel particle with $d_p=6$ mm and $D_{pipe}=45$ mm. **d** alumina particle with $d_p=6$ mm and $D_{pipe}=45$ mm. **e** aluminum particle with $C_p=62$. **f** alumina particle with $C_p=62$

3.2.6 Effect of particle shape

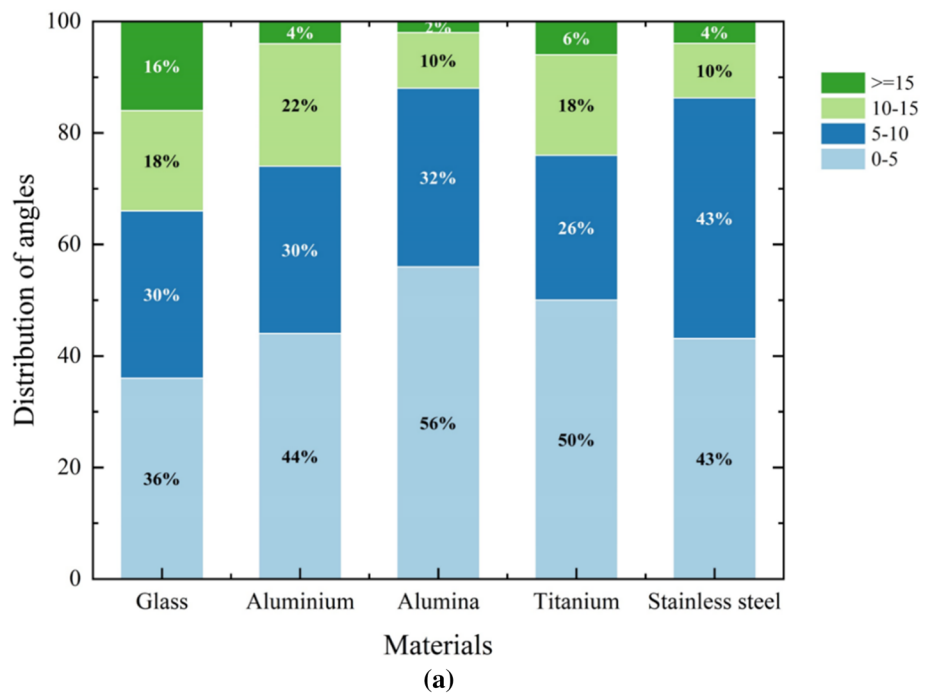
To investigate the influence of the particle shape on jamming, experiments with aluminum and alumina particles of different shapes (spherical and non-spherical) were conducted. Figure 5e, f present the variations in jamming probability with different shapes for aluminum and alumina, respectively. When the particle shape changed from spherical to non-spherical, the jamming probability for the two types of particles increased. These findings are understandable because when using non-spherical particles, there are additional particle–particle collisions and friction caused by roughness and eccentricity [36], increasing the ease with

which particle flow can form an arch; thus, jamming occurs. Although the volume-equivalent diameters of spherical and non-spherical particles are different, this result is convincing at a certain point because, as mentioned in Sect. 3.2.1, particle size has little effect on jamming probability. In addition, the differences between the volume-equivalent diameters of aluminum and alumina were small.

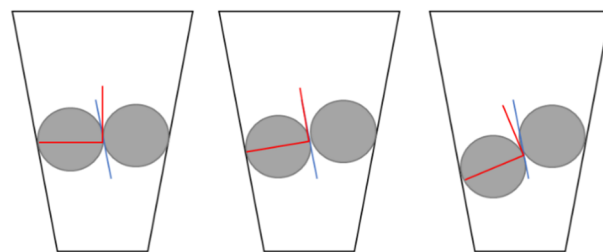
3.3 Analysis of arch stability

Figure 6b shows three types of blockage cases where the angles between the horizontal line and the line that connected two particles' centers (noted as α) were generally

Fig. 6 (Color online) Effect on the angle α . **a** Distribution of α for all spherical particles. **b** Different angles between the horizontal line and the line connected two particles' centers. The orange line is a horizontal line. **c** Three states for arches for different α . Blue line is parallel to left edge of the reducer pipe. Two red lines are the line crossing the center of particle and the tangent line of two circles



(b)



(i) stable state

(ii) critical state

(iii) unstable state

(c)

small. We analyzed five cases of different materials of particles (where each case has been repeated 50 times) and demonstrated that angle α in the majority (80%) of cases was less than 15° as shown in Fig. 6a. This finding corresponds with that of Kiwing et al. [19], who conducted experiments by releasing particles from a two-dimensional hopper. However, limited studies have investigated the arch angle. Three states for an arch, stable, critical, and unstable, were inferred, as shown in Fig. 6c. If α is small, the direction of static friction of two particles will be limited in the scope between the blue line and the tangent line, which makes the arch stable. When α increases, the arch enters a critical state where a heavy strike would break the arch. When α becomes so large that the tangent line becomes more inclined than the blue line, the arch enters an unstable state where a light impact would probably destroy the arch. This phenomenon suggests that observing the blockage with a small α is more likely than observe observing the blockage with a big α in the experiments.

4 Concluding remarks

Research on the process of flow blockage formation is critical for the safety analysis of LMFRs. To clarify the mechanisms of this behavior, in this study (first stage of the project), a series of experiments were conducted by releasing particles from a certain height into a reducer pipe. Because the primary target of our first stage is the effect of particle properties (rather than the subchannel shape) on blockage formation mechanisms, a reducer pipe with a circular cross-section is employed to simulate the subchannel of a fast reactor, and materials with different physical properties (e.g., size, capacity, and static friction coefficient) are utilized to simulate various sources of particles in flow blockage accidents. Observations and analyses in the literature have found that a jamming event is the result of the formation of an arch, which is closely related to the experimental parameters in this work. The parametric analyses reveal that under the present experimental conditions, the particle size, particle static friction coefficient, particle capacity, particle release pipe diameter, particle release height, and particle shape significantly influence the jamming probability. Specifically, the following results were obtained:

- First, the ratio of the outlet size of the reducer pipe to the particle diameter may be a determining factor for the occurrence of blockages. When the ratio of the outlet size to particle size was larger than R_c (in our experiment, $R_c = 6$), jamming did not occur. However, when the ratio was less than R_c , the jamming probability was not affected.
- Increasing the particle capacity or particle release pipe diameter led to an increase in particle number density, resulting in an increase in jamming probability. However, when the height the particles are released from increases, the jamming probability decreases due to the smaller particle number density and larger momentum of particles.
- In addition, static friction coefficient increases, jamming probability increases because the great tangential forces (i.e., static friction) make the arch system stable.
- Finally, non-spherical particles case lead to more particle–particle collisions and friction caused by the roughness and eccentricity than that in spherical particles case, which increases the jamming probability.

In further research, empirical models combining P_{arch} and the experimental parameters should be developed. In addition, our experiments with particle static friction coefficients, and those with particles of different polydispersities, could be enriched to improve the understanding of jamming. Moreover, numerical simulations could be conducted to investigate the flow blockage under more complicated conditions than those in this study. The knowledge and evidence from our experiments can be utilized to improve the design of the subchannel of the LMFRs, as well as the verification of computer models in fast reactor safety analysis codes.

Author contributions All authors contributed to the study conception and design. Material preparation, data collection and analysis were performed by Wen-Hui Jin, Song-Bai Cheng and Xiao-Xing Liu. The first draft of the manuscript was written by Wen-Hui Jin and all authors commented on previous versions of the manuscript. All authors read and approved the final manuscript.

Data availability The data that support the findings of this study are openly available in Science Data Bank at <https://www.doi.org/10.57760/sciencedb.j00186.00033> and <https://cstr.cn/31253.11.sciencedb.j00186.00033>.

Declarations

Conflict of interest The authors declare that they have no competing interests.

References

1. Y. Gao, Y. Zhu, Analysis of the influence on environmental radiation level of Qinshan area caused by Fukushima nuclear accident. *Nucl. Sci. Tech.* **25**, S010606 (2014). <https://doi.org/10.13538/j.1001-8042/nst.25.S010606>
2. T. Zhang, S. Cheng, T. Zhu et al., A new experimental investigation on local fuel-coolant interaction in a molten pool. *Ann. Nucl. Energy* **120**, 593–603 (2018). <https://doi.org/10.1016/j.anucene.2018.06.031>
3. S. Cheng, H. Yamano, Y. Suzuki et al., Characteristics of self-leveling behavior of debris beds in a series of experiments. *Nucl. Eng. Technol.* **45**(3), 323–334 (2013). <https://doi.org/10.5516/NET.02.2012.068>

4. G. Yang, H. Liao, T. Ding et al., Development and validation of a new oxide fuel rod performance analysis code for the liquid metal fast reactor. *Nucl. Sci. Tech.* **33**(5), 66 (2022). <https://doi.org/10.1007/s41365-022-01045-7>
5. X. Luo, C. Wang, Z. Zou et al., Development and application of a multi-physics and multi-scale coupling program for lead-cooled fast reactor. *Nucl. Sci. Tech.* **33**, 18 (2022). <https://doi.org/10.1007/s41365-022-01008-y>
6. W.S. Duan, Z. Zou, X. Luo et al., Startup scheme optimization and flow instability of natural circulation lead-cooled fast reactor SNCLFR-100. *Nucl. Sci. Tech.* **32**, 133 (2021). <https://doi.org/10.1007/s41365-021-00970-3>
7. X. Luo, L. Cao, W. Feng et al., Development of a subchannel code for blockage accidents of LMFBRs based on the 3D fuel rod model. *Nucl. Sci. Tech.* **33**(2), 27 (2022). <https://doi.org/10.1007/s41365-022-01010-4>
8. K. Shi, S. Li, X. Zhang et al., Partial flow blockage analysis of the hottest fuel assembly in SNCLFR-100 reactor core. *Nucl. Sci. Tech.* **29**, 16 (2018). <https://doi.org/10.1007/s41365-017-0351-3>
9. J.T. Han (ed.), *Blockages in LMFBF Fuel Assemblies: A Review of Experimental and Theoretical Studies* (ERDA, USA, 1977). <https://doi.org/10.2172/7301883>
10. K.V. Tichelen, *Blockages in LMFR Fuel Assemblies* (SCK CEN, Belgium, 2012)
11. K. Natesan, K. Velusamy, P. Selvaraj et al., Thermal hydraulic study on detection of random failure of fuel by delayed neutron detection system. *Nucl. Eng. Des.* **237**(23), 2219–2231 (2007). <https://doi.org/10.1016/j.nucengdes.2007.03.045>
12. M. Adorni, A. Bousbia-Salah, T. Hamidouche et al., Analysis of partial and total flow blockage of a single fuel assembly of an MTR research reactor core. *Ann. Nucl. Energy.* **32**(15), 1679–1692 (2005). <https://doi.org/10.1016/j.anucene.2005.06.001>
13. I. Di Piazza, M. Fabrizio, T. Mariano et al., A CFD analysis of flow blockage phenomena in ALFRED LFR demo fuel assembly. *Nucl. Eng. Des.* **276**, 202–215 (2014). <https://doi.org/10.1016/j.nucengdes.2014.05.033>
14. M. Sarkar, K. Velusamy, P. Munshi et al., Investigation of heat transfer from a totally blocked fuel subassembly of fast breeder reactor with 7 and 19 pin bundles. *Nucl. Eng. Des.* **338**, 74–91 (2018). <https://doi.org/10.1016/j.nucengdes.2018.08.001>
15. I. Di Piazza, R. Marinari, N. Forgiione, et al., CFD analyses of the internal blockage in the NACIE-UP fuel pin bundle simulator, in *Paper Presented at the 17th International Topical Meeting on Nuclear Reactor Thermal Hydraulics NURETH-17*, Xi'an Jiaotong University, Xi'an, 3–8 September 2017
16. R. Marinari, I. Di Piazza, N. Forgiione et al., Pre-test CFD simulations of the NACIE-UP BFPS test section. *Ann. Nucl. Energy.* **110**, 1060–1072 (2017). <https://doi.org/10.1016/j.anucene.2017.08.046>
17. J. Pacio, M. Daubner, F. Fellmoser et al., Heat transfer experiment in a partially (internally) blocked 19-rod bundle with wire spacers cooled by LBE. *Nucl. Eng. Des.* **330**, 225–240 (2018)
18. R. Marinari, I. Di Piazza, M. Tarantino et al., Blockage fuel pin simulator experiments and simulation. *Nucl. Eng. Des.* **353**, 110215 (2019). <https://doi.org/10.1016/j.nucengdes.2019.110215>
19. T. Kiwing, Y.L. Pik, H.K. Pak, Jamming of granular flow in a two-dimensional hopper. *Phys. Rev. Lett.* **86**(1), 71–74 (2001)
20. I. Zuriguel, A. Garcimartin, D. Maza et al., Jamming during the discharge of granular matter from a silo. *Phys. Rev. E* **71**, 051303 (2005). <https://doi.org/10.1103/PhysRevE.71.051303>
21. I. Zuriguel, L. Pughaloni, A. Luis et al., Jamming during the discharge of grains from a silo described as a percolating transition. *Phys. Rev. E.* **68**, 030301 (2003). <https://doi.org/10.1103/PhysRevE.68.030301>
22. J. Sienicki, in *Lead-Cooled Fast Reactors*. ed. by A. Waltar, D. Todd, P.V. Tsvetkov (Springer, Boston, 2012). https://doi.org/10.1007/978-1-4419-9572-8_18
23. F.S. Craig, G.H. William, W.B. Neil et al., SSTAR: the US lead-cooled fast reactor (LFR). *J. Nucl. Mater.* **376**, 255–259 (2008). <https://doi.org/10.1016/j.jnucmat.2008.02.049>
24. F. Roelofs (ed.), *Thermal Hydraulics Aspects of Liquid Metal Cooled Nuclear Reactors* (Woodhead Publishing, London, 2018), pp.17–47. <https://doi.org/10.1016/B978-0-08-101980-1.00003-X>
25. S. Cheng, P. Gong, S. Wang et al., Investigation of flow regime in debris bed formation behavior with nonspherical particles. *Nucl. Eng. Technol.* **50**, 43–53 (2018). <https://doi.org/10.1016/j.net.2017.09.003>
26. P.C. Arnold, A.G. McLean, An analytical solution for the stress function at the wall of a converging channel. *Powder Technol.* **13**(2), 255–260 (1976). [https://doi.org/10.1016/0032-5910\(76\)85011-5](https://doi.org/10.1016/0032-5910(76)85011-5)
27. A. Drescher, A.J. Waters, C.A. Rhoades, Arching in hoppers: ii. Arching theories and critical outlet size. *Powder Technol.* **84**(2), 177–183 (1995). [https://doi.org/10.1016/0032-5910\(95\)029828](https://doi.org/10.1016/0032-5910(95)029828)
28. W. Jenike, Steady gravity flow of frictional-cohesive solids in converging channels. *J. Appl. Mech.* **31**(1), 5–11 (1964). <https://doi.org/10.1115/1.3629571>
29. D.M. Walker, An approximate theory for pressures and arching in hoppers. *Chem. Eng. Sci.* **21**(11), 975–997 (1966). [https://doi.org/10.1016/0009-2509\(66\)85095-9](https://doi.org/10.1016/0009-2509(66)85095-9)
30. R.A. Meyers (ed.), *Statistical Mechanics of Clogging* (Springer, Berlin, 2020). https://doi.org/10.1007/978-3-642-27737-5_746-1
31. A. Janda, I. Zuriguel, A. Garcimartin et al., Jamming and critical outlet size in the discharge of a two-dimensional silo. *Europhys. Lett.* **84**(4), 44002 (2008). <https://doi.org/10.1209/02955075/84/44002>
32. L. Pournin, M. Ramaioli, P. Folly et al., About the influence of friction and poly-dispersi-tyon the jamming behavior of bead assemblies. *Eur. Phys. J. E.* **23**(2), 229–235 (2007). <https://doi.org/10.1140/epje/i2007-10176-5>
33. L.A. Pughaloni, M.G. Valluzzi, L.G. Valluzzi, Arching in tapped deposits of hard disks. *Phys. Rev. E.* **73**, 051302 (2006). <https://doi.org/10.1103/physreve.73.051302>
34. G.A. Kohring, S. Melin, H. Puhl et al., Computer simulations of critical, non-stationary granular flow through a hopper. *Comput. Methods Appl. Mech. Eng.* **124**(3), 273–281 (1995). [https://doi.org/10.1016/0045-7825\(94\)00743-7](https://doi.org/10.1016/0045-7825(94)00743-7)
35. M. Hou, W. Chen, T. Zhang et al., Global nature of dilute-to-dense transition of granular flows in a 2d channel. *Phys. Rev. Lett.* **91**(20), 204301 (2003). <https://doi.org/10.1103/PhysRevLett.91.204301>
36. S. Cheng, H. Tagami, H. Yamano et al., An investigation on debris bed self-leveling behavior with non-spherical particles. *J. Nucl. Sci. Technol.* **51**, 1096–1106 (2014). <https://doi.org/10.1080/00223131.2014.910478>

Springer Nature or its licensor (e.g. a society or other partner) holds exclusive rights to this article under a publishing agreement with the author(s) or other rightsholder(s); author self-archiving of the accepted manuscript version of this article is solely governed by the terms of such publishing agreement and applicable law.